

Communication

Digital Reconfiguration of a Single Arm 3-D Bowtie Antenna

Fatima A. Asadallah¹, Aline Eid², Ghida Shehadeh, Joseph Costantine¹,
Youssef Tawk¹, and Emmanouil M. Tentzeris³

Abstract—This communication proposes the reconfiguration of a coplanar-fed single arm bowtie antenna structure by relying on the integration of a digital tunable capacitor (DTC). The coplanar-fed single arm bowtie antenna is presented in two configurations. The first configuration is a 2-D topology with a modified ground plane arrangement. The second configuration employs vertical folding for the ground plane as well as the radiating arm. In addition, vertical copper inserts are embedded within the bowtie single arm to further enhance the compactness of the structure and transform it into a 3-D topology. Both antennas are initially designed to operate at 868 MHz for Internet of Things (IoT) applications, with a digitally reconfigurable frequency operation for wireless communication. The 2-D antenna structure exhibits a 77% size reduction at the IoT operational frequency of 868 MHz in comparison with a similar rectangular patch antenna operating at the same frequency. On the other hand, the 3-D antenna structure reaches 84% of size reduction at the same frequency. A figure of merit (FOM) is derived to prove the superior performance of the presented antenna structure.

Index Terms—Bowtie antenna, compact antenna, digital tunable capacitor (DTC), Internet of Things (IoTs), planar antenna, reconfigurable antenna.

I. INTRODUCTION

The integration of reconfigurable antennas in modern communication systems requires the digitization of their control circuitry in order to enable an easier and more agile platform. On the other hand, reconfiguring a miniaturized and compact antenna structure requires additional care in order to reduce the impact of the reconfiguration technique on the antenna performance. While several reconfiguration techniques have been proposed in literature [1], [2], digital reconfiguration presents a low power-consuming alternative, while enabling an easier software control [3], [4].

A reconfigurable antenna that caters to modern wireless communication applications must be able to conform to its platform. A variety of antenna topologies can be adopted [5], [6] whether 2-D or 3-D in order to better satisfy any device integration constraint. To that extent, in this communication, a compact digitally reconfigurable coplanar-fed single arm bowtie antenna is presented for integration into an Internet of Things (IoTs) platform. The antenna is proposed in two embodiments. The first topology is a 2-D structure with an ability to conform into any planar surface. The second topology that was briefly introduced in [4] in its simulated design is fabricated

Manuscript received July 8, 2020; revised November 22, 2020; accepted November 28, 2020. Date of publication December 21, 2020; date of current version July 7, 2021. This work was supported by the American University of Beirut University Research Board. (Corresponding author: Joseph Costantine.)

Fatima A. Asadallah, Ghida Shehadeh, Joseph Costantine, and Youssef Tawk are with the Electrical and Computer Engineering Department, American University of Beirut, Beirut 1107 2020, Lebanon (e-mail: jcostantine@ieee.org).

Aline Eid and Emmanouil M. Tentzeris are with the School of Electrical and Computer Engineering, Georgia Institute of Technology, Atlanta, GA 30332 USA.

Color versions of one or more figures in this communication are available at <https://doi.org/10.1109/TAP.2020.3044703>.

Digital Object Identifier 10.1109/TAP.2020.3044703

0018-926X © 2020 IEEE. Personal use is permitted, but republication/redistribution requires IEEE permission.

See <https://www.ieee.org/publications/rights/index.html> for more information.

herein along its biasing network and digital control. The discussion of both topologies in this communication also includes a detailed analysis of the measurement, performance, and superior characteristics. These topologies present novel more compact prototypes that enable their implementation into a smaller IoT platform whether planar or volumetric. Both topologies target the Long Range (LoRa) Europe and US bands (868 and 915 MHz), Global System for Mobile Communications (GSM) (1.8 GHz), and Long Term Evolution (LTE) (2.1 GHz) bands by relying on a single digital tunable capacitor (DTC) [7].

The integration of compact frequency reconfigurable antennas is needed in IoT devices in order to enable their operation across the various frequency bands with acceptable performance characteristics. As an example, Asadallah *et al.* [4] present a digitally reconfigurable miniaturized inverted F-antenna for IoT integration to cater for a variety of applications. On the other hand, Castro and Sharma [6] present a flexible circularly polarized antenna that can be integrated on any curved surface for efficient communication.

Several aspects identify the novelty of this communication. The first aspect is based on the ability of this antenna to transition from 2-D to 3-D structure without impacting its radiation characteristics while enhancing its compactness. The second factor relates to the fact that digital reconfiguration is achieved by relying on a single DTC that enables the antenna in all its topologies to cater for IoT communication requirements. The 3-D antenna structure, on the other hand, employs a volumetric folding mechanism that drastically reduces the size of the antenna. Such volumetric restructuring resorts to the integration of vertical folds in addition to conductive-based vertical inserts at strategic locations.

Section II of this communication presents the design process of the 2-D frequency reconfigurable antenna, whereas Section III presents the transition to the 3-D structure. Section IV presents the measurement results along with a figure of merit (FOM) analysis. The communication is finally concluded in Section V.

II. SINGLE ARM 2-D RECONFIGURABLE BOWTIE DESIGN

The presented antenna is a single arm bowtie structure that adopts a coplanar waveguide (CPW) feeding mechanism. The proposed structure is shown in Fig. 1 where the ground is composed of two distinct sections. The first section is a rectangular metallic part of dimensions 50 mm × 18 mm, while the second one has a triangular shape with dimensions indicated in Fig. 1. The two ground sections are designed to enhance the antenna's radiation behavior by ensuring a well-balanced return path for the current's flow. In addition, such feeding mechanism allows the removal of one of the two bowtie arms while simultaneously contributing to the remaining bowtie arm's radiation mechanism additively and constructively. Such topology allows the antenna to resonate at 868 MHz with a realized gain of 4.1 dB. The adoption of a CPW feeding with an optimized ground dimensions guarantees a compact size with overall area dimensions of 50 mm × 70 mm accordingly.

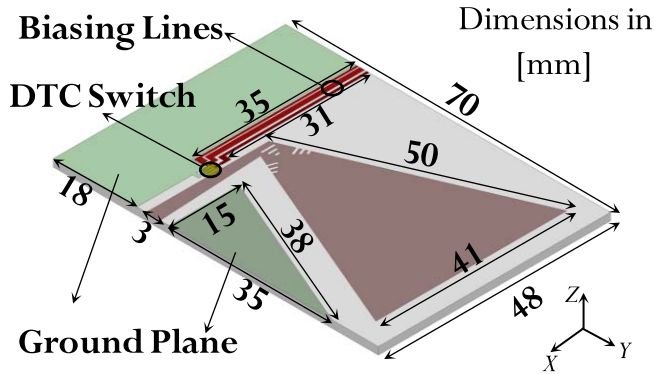


Fig. 1. Layout of 2-D single arm bowtie antenna.

The overall structure of the proposed antenna lies on the top layer of an Ultralam substrate with a dielectric constant of 2.9 and a loss tangent of 0.022 ($\tan \delta = 0.022$). Such topology features a 2-D property where both the antenna’s radiating single bowtie arm as well as the two ground sections are incorporated along the same plane. To enable the frequency reconfiguration of the antenna, a DTC (Part # Pe64907, Peregrine Semiconductor [7]) is strategically located along the feeding line as highlighted in Fig. 1. More specifically, the DTC is placed in a shunt position on the feeding line in order to dynamically tune the input impedance of the antenna. Three slot arrays are etched out of the bowtie arm in order to adjust the input impedance in conjunction with the changing configurations of the DTC.

The digital control of the 5-bit binary input allows the tuning of the capacitance. Accordingly, 32 ($2^5 = 32$) different capacitance values (or states) can be obtained through such control. The modeling of the DTC component accounts for its constant inductive effect of 0.7 nH and its variable capacitance as well as resistance for different digital control inputs [7]. Such control is obtained through the incorporation of three distinct high impedance biasing lines of width 0.5 mm each as presented in Fig. 1. These biasing lines are placed next to the rectangular ground plane and separated by a small gap of 0.5 mm, respectively. These three biasing lines are required to provide the connection between the DTC’s three serial peripheral interfaces (SPIs) and the microcontroller that provides the digital control. The three SPIs are the clock input, the latch enable input, and the data input. As a result, the DTC changes its capacitance and resistance accordingly when the serial interface clock input is fed by a clock of 38.4 ns and the serial interface latch enable input is fed by a rising pulse.

At the end of each biasing line, a 110 nH RF choke is included. These chokes prevent the RF leakage from going back into the microcontroller that controls the DTC. In this communication, the Nucleo-RL54 microcontroller is used to control the 32 states that govern the DTC operation by supplying the corresponding 5 bits sequence. For example, in state 0, the DTC has a capacitance of 0.85 pF, a resistance of 0.7 Ω , and an inductance of 0.7 nH, while in state 31, the DTC achieves a capacitance of 2.586 pF, a resistance of 1.33 Ω , and an inductance of 0.7 nH [7].

As a result, when the DTC is in state 0, the antenna operates at 1.2 and 2.1 GHz. Then, the antenna shifts its frequency operation as the DTC state increases to reach state 20 where the original operating frequency at 868 MHz is recovered. The change in the antenna’s reflection coefficient for various states is shown in Fig. 2. The co- and cross-polarization of the radiation patterns of the antenna for different states are presented in Fig. 3. An additional feature that this antenna exhibits is producing different radiation patterns for different frequency operations. Each of these patterns caters for the application of the antenna at that particular frequency of operation.

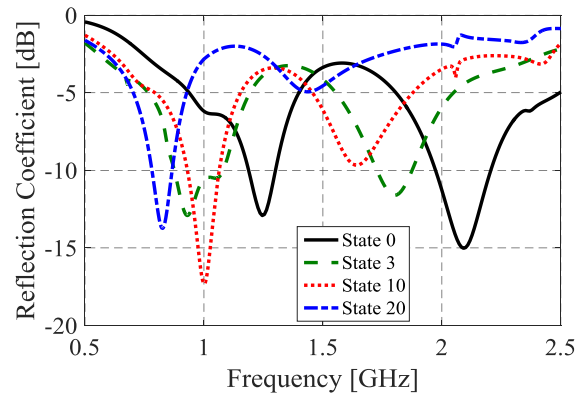


Fig. 2. Change in the reflection coefficient of the 2-D single arm bowtie antenna for different DTC states.

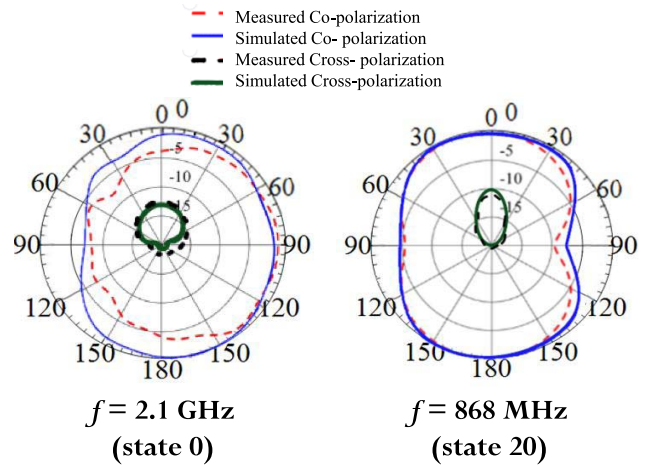


Fig. 3. Radiation patterns of the 2-D single arm antenna at $\phi 0^\circ$ (solid line) and $\phi 90^\circ$ (dotted line) for two distinct frequencies.

TABLE I
ANTENNA RADIATION EFFICIENCY, GAIN, AND SIZE REDUCTION FOR DIFFERENT OPERATIONAL FREQUENCIES AND STATES

Frequency [GHz]	State	Radiation Efficiency (%)	Size Reduction (%)	Gain [dB]	BW [MHz]
0.868	20	78	77	4.1	100
0.915	3	86	75	4.5	200
1	10	84	73	4.9	200
1.8	3	87	25	5.6	200
2.1	0	92	0	6	250

For example, at the industrial, scientific and medical (ISM) bands (868 MHz), an omnidirectional pattern is obtained as required for IoT communication. As for LTE and GSM bands (2.1 and 1.8 GHz), the structure produces an endfire pattern that is suitable for long distance communication. These patterns ensure the versatile functionality of the antenna across a multitude of bands as required for modern IoT devices. The various electrical properties of the presented antenna structure at different states are summarized in Table I. For example, a 92% radiation efficiency (RE) with a gain of 6 dB is obtained at 2.1 GHz. This is realized when the DTC is in state 0. The DTC is a combination of variable resistance and capacitance. The equivalent circuit of the DTC is a combination of a variable resistance and capacitance. We believe that the change in bandwidth, gain,

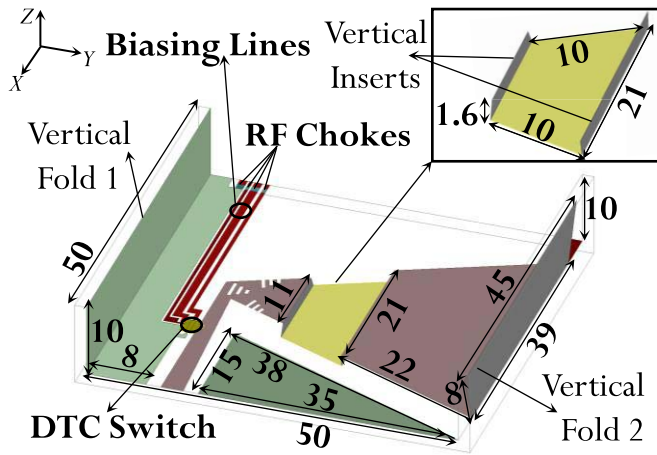


Fig. 4. 3-D single arm bowtie antenna structure.

and efficiency is related to change in the input impedance. As the state number increases, the DTC equivalent resistance increases thus leading to an increase in the power dissipated inside the DTC. This power loss will reduce the power accepted by the antenna and thus will reduce both the antenna gain and efficiency. Furthermore, the bandwidth change is a direct consequence in the change of the input impedance.

At 1.8 GHz (state 3), the antenna produces an RE of 87%. Such drop is due to the increase in the capacitance and ohmic losses of the DTC. The other states allow the antenna to tune its operational frequency with a gain reaching 4.1 dB at state 20 with a resonant frequency of 868 MHz, respectively. At this frequency, a size reduction of 77% is achieved in comparison with a rectangular microstrip patch antenna resonating at the same frequency. The DTC requires 2.75 V dc voltages with a 140 μ A dc current [7]. Therefore, the DTC consumes an average of 385 μ W as its dc power consumption.

III. SINGLE ARM 3-D RECONFIGURABLE BOWTIE DESIGN

The size of the 2-D antenna structure discussed in Section II can be further reduced to achieve a more compact design. The additional size reduction is obtained by modifying the antenna's layout from a 2-D perspective to a 3-D one. Such task relies on integrating several modifications to the 2-D antenna structure presented in Section II.

The first modification includes the incorporation of two vertical folds to the antenna's layout as highlighted in Fig. 4. The first vertical fold is connected to the antenna's rectangular ground plane. Such folding ensures that the same 18 mm width for the rectangular ground plane is maintained. However, this width is now divided into two parts. The first part remains in the original 2-D plane of the antenna with a width of 8 mm, while the second part is aligned orthogonally with a height of 10 mm along the z-axis. The second fold is also based on vertically extending the bowtie single arm along the z-axis over a distance of 8 mm. These two vertical folds reduce the antenna's overall dimensions from 70 mm \times 50 mm to 50 mm \times 50 mm.

The incorporation of the two vertical folds leads to a drastic mismatch at the design frequencies. This is due to the reactive loading of the vertical folds on the antenna's input impedance. To quantify such effect, the antenna's input impedance is monitored without having a DTC integrated along the feeding line. Accordingly, the corresponding antenna's input impedance is shifted from 50 Ω to 19 + j50 Ω at 868 MHz and to 88. -j121 Ω at 2.1 GHz, as shown in Fig. 5.

In order to cancel out such reactive effect, two different techniques are adopted simultaneously. The first technique is based on

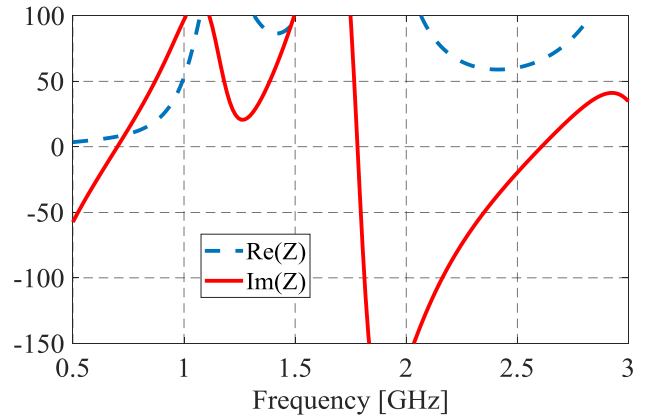


Fig. 5. Antenna's input impedance after incorporating the two vertical folds and without integrating a DTC.

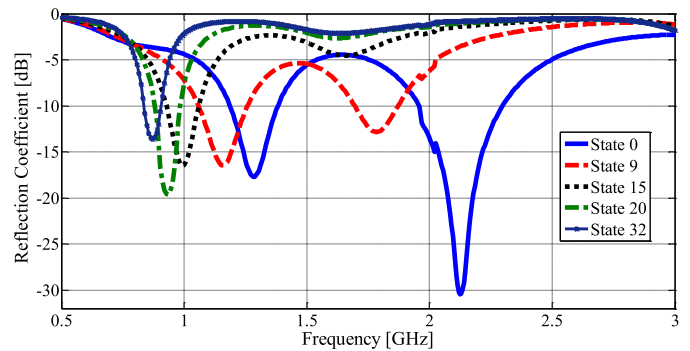


Fig. 6. Change in the 3-D antenna's reflection coefficient after adding the two vertical folds and the two vertical copper inserts.

incorporating a DTC along the antenna's feeding line. The job of the DTC is to provide the appropriate capacitive effect at 868 MHz while supplying an inductive effect at 2.1 GHz. Furthermore, the variation of the DTC states cancels the imaginary parts of the input impedances at different frequencies. This is accompanied by the incorporated slot arrays that are adopted from the 2-D topology. Hence, a reconfigurable impedance matching at the desired frequencies of operation is achieved.

The second technique is based on folding the bowtie single arm along the negative z-axis. Accordingly, two vertical copper inserts are added to the antenna structure as presented in Fig. 4. The objective of these inserts is to connect the antenna substrate's top layer to its bottom layer. Such modification allows the antenna's single arm to fold along the two sides of the substrate. The first rectangular insert has a length of 11 mm, while the second one is designed with a length of 21 mm. The folding of the bowtie's single arm enhances the antenna's impedance matching at the various states of the incorporated DTC as summarized in the simulated reflection coefficient results in Fig. 6 for various states. The same biasing technique is adopted where three high impedance lines are embedded within the antenna structure and terminated by 110 nH RF chokes.

IV. MEASUREMENT RESULTS

The antenna structure is fabricated and assembled, as shown in Fig. 7(a). Conductive adhesives are used to connect the two vertical folds and the two vertical inserts to the various antenna parts. By taking as a reference a microstrip antenna design operating at the lowest design frequency of 868 MHz, the proposed structure

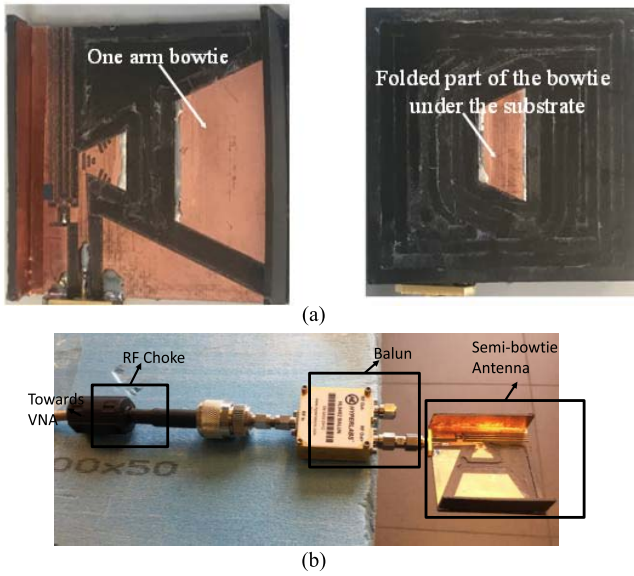


Fig. 7. (a) Top and bottom layers of the fabricated 3-D design. (b) Small antenna measurement technique.

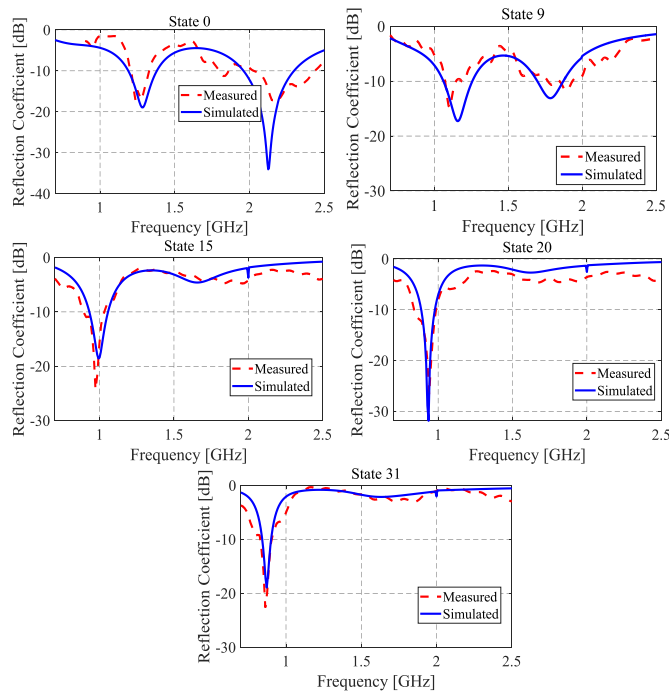


Fig. 8. Simulated and measured reflection coefficient for different DTC states.

exhibits an overall 84% size reduction. Therefore, small antenna measurement techniques must be implemented in order to ensure accurate results [8], [9]. More specifically, a ferrite bead RF Choke is cascaded with the coaxial cable in order to decrease the RF leakage, as shown in Fig. 7(b).

In addition, a balun is used as a part of the small antenna measurements technique. It electrically isolates the antenna's current path from the coaxial cable and thus minimizes the effects of the cable on the small antenna.

The comparison between the simulated and measured reflection coefficient results for different states of the DTC is shown in Fig. 8.

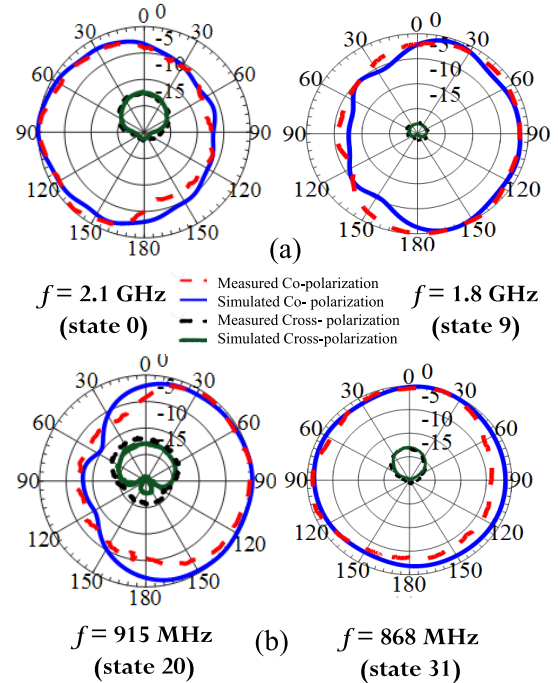


Fig. 9. Simulated and measured radiation patterns at (a) $\phi = 0^\circ$ and (b) $\phi = 90^\circ$.

TABLE II
ANTENNA RADIATION EFFICIENCY AND SIZE REDUCTION FOR VARIOUS DTC STATES ALONG WITH ITS CORRESPONDING FREQUENCY

Frequency [GHz]	State	Size Reduction (%)	Radiation Efficiency (%)	Gain [dB]	BW [MHz]
0.868	31	84	88	0.19	90
0.915	20	82	87	0.41	140
1	15	80	84	0.78	200
1.8	9	32	95	1.7	200
2.1	0	0	97	3.17	400

All simulated data rely on Ansys Electronic Desktop [10]. The fabricated prototype is able to reconfigure its operating bandwidth for the various states of the integrated DTC. The co- and cross-polarization of the simulated and measured radiation patterns for the proposed design are presented in Fig. 9(a) for $\phi = 0^\circ$ and in Fig. 9(b) for $\phi = 90^\circ$ at different frequencies. It can be noticed that the cross-polarization level (CPL) varies between 10 and 25 dB over different frequencies. This proves that the antenna is linearly polarized over all its frequencies of operation. A good agreement is noticed between the simulated and measured results for various frequencies along both planes.

Table II presents the antenna RE and size reduction for different DTC states. The antenna's RE at 2.1 GHz is 97% with a realized gain of 3.17 dB. At 1.8 GHz, the antenna produces an RE of 96% with a size reduction of almost 32% in comparison with a typical $\lambda/2$ patch at 1.8 GHz. At state 20, the RE is found to be 87% at 915 MHz with a size reduction of almost 82% in comparison with a typical rectangular Microstrip antenna operating at the same frequency with

TABLE III
COMPARATIVE TABLE BETWEEN THE PROPOSED
DESIGN AND LITERATURE

	Size	# Switches	Rad. Eff. (%)	FOM
[3]	0.19λx0.04λ	1	60%@960MHz 25%@600MHz	32
[11]	0.145λx0.13λ	3	52%@1.5GHz	31
[12]	0.15λx0.09λ	2	50%@700MHz	30
[13]	0.17λx0.1λ	2	10%@2.4GHz 65%@3.5GHz	5.88
[14]	1.28λx1.28λ	4	75%@2.25GHz 66%@2.25GHz	1
This work	0.14λx0.14λ	1	85%@868MHz 84%@915MHz 84%@1GHz 95%@1.8GHz 97%@2.1GHz	42.85

a gain around 0.4 dB. In addition, at state 32, the RE is found to be 88% at 868 MHz with a gain that is equal to 0.19 dB and a size reduction of 84% in comparison with a typical patch operating at the same frequency. The decrease in the antenna size, and the high capacitance and resistance values of the DTC in states ranging between 20 and 31 impact the RE and gain of the antenna.

The compactness and efficiency of the proposed antenna are finally benchmarked using the below FOM which is the RE per unit of electrical area (area normalized to the effective wavelength at the operating frequency of the antenna). Its equation is shown in the following equation:

$$FOM = \frac{RE}{100 \times V_{normalized}}$$

$$\text{With } V_{Normalized} = \frac{Volume_{Antenna}}{\lambda_3} \text{ and } \lambda = \frac{c}{\sqrt{\epsilon_r} * f}. \quad (1)$$

The FOM of the proposed antenna is calculated and included in Table III for comparison with available antenna structures in the literature [3], [11]–[14]. The dimensions are expressed as a function of the largest wavelength. Table III highlights the outperformance of the proposed technique and design architecture. Such performance is highlighted by maintaining both high efficiency values despite the high compactness aspect of the antenna structure. The presented structure herein features the highest FOM with the smallest number of switches while covering different operating frequencies.

V. CONCLUSION

Frequency reconfigurable single arm 2-D and 3-D bowtie designs are proposed in this communication. The antennas are proposed for

IoT devices integration and resort to only one DTC in order to operate at the required frequency bands. The antennas also present 77% and 88% size reduction at 868 MHz. The conversion from a 2-D to a 3-D topology is obtained through the integration of vertical folds as well as copper-based vertical inserts. Such integration enables a size reduction of 84% in comparison with a patch antenna operating at 868 MHz. An FOM is presented to prove the superior performance of the proposed antenna structure in terms of high miniaturization aspect and enhanced RE.

REFERENCES

- [1] J. Costantine, Y. Tawk, S. E. Barbin, and C. G. Christodoulou, "Reconfigurable antennas: Design and applications," *Proc. IEEE*, vol. 103, no. 3, pp. 424–437, Mar. 2015.
- [2] L. Sh Chen *et al.*, "Pattern-reconfigurable antenna with five switchable beams in elevation plane," *IEEE Antennas Wireless Propag. Lett.*, vol. 17, no. 3, pp. 454–457, Mar. 2018.
- [3] T. Houret, L. Lizzi, F. Ferrero, C. Danchesi, and S. Boudaud, "DTC-enabled frequency-tunable inverted-F antenna for IoT applications," *IEEE Antennas Wireless Propag. Lett.*, vol. 19, no. 2, pp. 307–311, Feb. 2020.
- [4] F. A. Asadallah, J. Costantine, and Y. Tawk, "A digitally tuned reconfigurable semi-bowtie antenna for IoT devices," in *Proc. 12th Eur. Conf. Antennas Propag. (EuCAP)*, Apr. 2018, pp. 1–2, doi: 10.1049/cp.2018.0918.
- [5] B. K. Tehrani, B. S. Cook, and M. M. Tentzeris, "Inkjet printing of multilayer millimeter-wave yagi-uda antennas on flexible substrates," *IEEE Antennas Wireless Propag. Lett.*, vol. 15, pp. 143–146, 2016.
- [6] A. T. Castro and S. K. Sharma, "Inkjet-printed wideband circularly polarized microstrip patch array antenna on a PET film flexible substrate material," *IEEE Antennas Wireless Propag. Lett.*, vol. 17, no. 1, pp. 176–179, Jan. 2018.
- [7] P. Semiconductor. PE64907. Accessed: Oct. 14, 2020. [Online]. Available: <http://www.psemi.com/products/digitally-tunable-capacitors-dtc/pe64907>
- [8] 2018K. Fujimoto and H. Morishita, *Modern Small Antennas*. Cambridge, U.K.: Cambridge Univ. Press, 2013.
- [9] J. Volakis, C.-C. Chen, and K. Fujimoto, *Antennas: Miniaturization Techniques & Applications*, 1st ed. New York, NY, USA: McGraw-Hill, 2010.
- [10] *Ansys Electronic Desktop, Release 18.1, Help System, Far Field Analysis Guide*, ANSYS, Canonsburg, PA, USA, 2018.
- [11] N. Nguyen-Trong, A. Piotrowski, L. Hall, and C. Fumeaux, "A frequency- and polarization-reconfigurable circular cavity antenna," *IEEE Antennas Wireless Propag. Lett.*, vol. 16, pp. 999–1002, 2017.
- [12] G. Chaabane, V. Madrangeas, M. Chatras, E. Arnaud, L. Huitema, and P. Blondy, "High-linearity 3-Bit frequency-tunable planar Inverted-F antenna for RF applications," *IEEE Antennas Wireless Propag. Lett.*, vol. 16, pp. 983–986, 2017.
- [13] A. Boukarkar, X. Q. Lin, Y. Jiang, L. Y. Nie, P. Mei, and Y. Q. Yu, "A miniaturized extremely close-spaced four-element dual-band MIMO antenna system with polarization and pattern diversity," *IEEE Antennas Wireless Propag. Lett.*, vol. 17, no. 1, pp. 134–137, Jan. 2018.
- [14] W. Lin, H. Wong, and R. W. Ziolkowski, "Wideband pattern-reconfigurable antenna with switchable broadside and conical beams," *IEEE Antennas Wireless Propag. Lett.*, vol. 16, pp. 2638–2641, 2017.